applied optics

Synchronous driving scheme for silicon-based optical switches to critically compensate for thermo-optic effect in carrier injection

Mingle Liao,[1] Baojian Wu,[1,*] Wei Huang,[1] Heng Zhou,[1] Linjie Zhou,[2] Kun Qiu,[1] and Jianping Chen[2]

[1]Key Lab of Optical Fiber Sensing and Communication Networks, Ministry of Education, University of Electronic Science and Technology of China, 611731 Chengdu, China
[2]State Key Laboratory of Advanced Optical Communication Systems and Networks, Department of Electronic Engineering, Shanghai Jiao Tong University, Shanghai 200240, China
*Corresponding author: bjwu@uestc.edu.cn

Received 23 September 2016; revised 2 December 2016; accepted 2 December 2016; posted 5 December 2016 (Doc. ID 276334); published 6 January 2017

The switching performance of high-speed optical-switching-integrated chips is to a great extent dependent on the carrier injection technique, which is accompanied by the thermo-optic effect. In this paper, we put forward a synchronous driving scheme for the silicon-based Mach–Zehnder interferometer (MZI) optical switches, which is capable of critically compensating for the temperature variation with carrier injection to the p-i-n diode on one arm of the MZI by applying a synchronous modulating voltage to the silicon resistive heater on the other MZI arm. The synchronous compensation mechanism is identified by experiments and simulation. Our experimental data show that, by comparison with the traditional driving scheme, the synchronous driving scheme can improve the extinction ratio by 1 dB, along with a better switching waveform.

OCIS codes: (130.0130) Integrated optics; (130.4815) Optical switching devices; (230.2090) Electro-optical devices; (120.6810) Thermal effects.

https://doi.org/10.1364/AO.56.000205

1. INTRODUCTION

Optical switching structure, as a bridge of connecting different input and output ports, plays a key role in both long-haul optical communications and short-reach optical interconnects [1,2]. In current networks, large-scale optical switching nodes are usually realized in the electrical domain through optical-electronic-optical (O-E-O) conversion. However, with the development of high-speed networks, this way is more and more limited by an electronic bottleneck, while all-optical switching technology is deemed to be an effective solution [3,4]. There are several approaches to configuring all-optical switches, such as micro-electro-mechanical systems (MEMS) [5,6], and silica planar light-wave circuits (PLC) [7,8]. Silicon-based electro-optic (EO) switching chips using the free-carrier plasma dispersion (FCD) effect have a potential application to high-speed all-optical networks due to short switching times in the nanosecond order of magnitude [9–12]. $N \times N$ optical switches are usually constructed by several 1×2 or 2×2 switch elements with a specific topological structure. Recently, 16×16 non-blocking optical switching silicon chips based on Mach–Zehnder interferometers (MZIs) or dual-ring assisted MZIs (DR-MZIs) have been developed [13]. The compensation for the fabrication errors can be done by two effective methods: those of applying a small electrical forward bias voltage [14], or adding thermo-optic tuners to both MZI arms [15,16].

However, the carrier injection process through the p-i-n diode for high-speed change of the refractive index will also be accompanied by an inevitable temperature rise since silicon is of high thermo-optical coefficient (1.86×10^{-4} K^{-1}) at room temperature. The influence of temperature variation on the switching performance can be reduced by optimizing the waveguide length or the electrode position [17] to a certain extent. In this paper, we put forward a synchronous driving scheme to compensate for the temperature variation with carrier injection. That is, the resistive heater on one arm of each 2×2 MZI switch is driven by a synchronous modulating signal, varying with the on–off voltages applied to the p-i-n diode on the other arm. The synchronous mechanism for thermal compensation is illustrated by experiments and simulation. To test and verify the idea, we designed a multi-port field-programmable gate array (FPGA) driver circuit for accurate control of the 4×4 silicon-based MZI optical switching chips. Our experimental results show that the synchronous driving scheme is capable of improving the extinction ratio (ER) by 1 dB compared to the traditional driving method, and that the corresponding switching waveform becomes better as well.

The rest of the paper is organized as follows. Section 2 analyzes the static and dynamic characteristics of a silicon-based MZI optical switch, which are carried out by simulation and calculation. Section 3 presents the experimental results of the device, which are identical with the theoretical results. Next, in Section 4, we identify the proposed scheme with experiments and calculation. Finally, we make our conclusions in Section 5.

2. CARRIER INJECTION AND THERMO-OPTIC CHARACTERISTICS OF SILICON-BASED MZI OPTICAL SWITCH

Silicon-based MZI optical switches are one of basic units of high-speed optical-switching-integrated chips. A typical silicon-based MZI structure, as shown in Fig. 1 [18], consists of two 2×2 multimode interferometers (MMIs) linked by two arms with p-i-n diodes for fast EO switching and silicon resistive heaters for fabrication error correction [16,19]. In our experiments and simulation, the following parameters are available. The cross-sectional dimension of the silicon ridge waveguides is 0.5 μm(width) × 0.22 μm(height) with a slab thickness of 60 nm. The lengths of the p-i-n diodes and the silicon resistive heaters are, respectively, $l_c = 356$ μm and $l_t = 89$ μm, corresponding to the driver voltages u_c and u_t (referring to Fig. 1). The doping concentration of the highly doped $p+$ and $n+$ regions is $\sim 10^{20}$ cm^{-3}, separated from the waveguide edges by 0.8 μm to avoid free carrier absorption (FCA) loss. The aluminum metal connection wires have ohmic contact with the two highly doped regions, and are finally wire-bonded to a printed circuit board (PCB) for electrical tuning of silicon-resistive heaters and the p-i-n diodes.

Assume that the two MMIs are ideal 3 dB couplers, and the transmissivity of the MZI optical switch from the input port I_1 to the output port O_1 can be expressed as

$$T = P_{1,\mathrm{out}}/P_{1,\mathrm{in}} = \frac{1}{4}\left[T_1 + T_2 - 2\sqrt{T_1 T_2}\cos(\Delta\varphi)\right], \quad (1)$$

where T_1 and T_2 are the power transmissivity of the two arms, and $\Delta\varphi$ is the phase difference of the two arms.

The MZI optical switch can operate at the best "OFF" (Cross) and "ON" (Bar) states when $\Delta\varphi = 0$ and π, respectively. To perfectly correct the fabrication errors, a bias voltage u_t is often applied to the silicon resistive heaters in the upper arm of the MZI switch. In the case when no voltage is applied

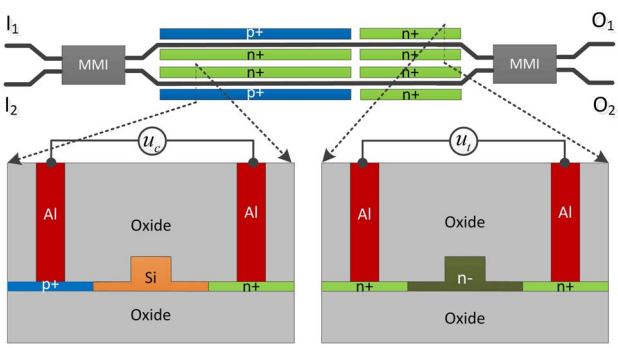

Fig. 1. 2×2 MZI switch element and the cross sections of the p-i-n diode and the silicon resistive heaters.

to the p-i-n diode, the MZI optical switch is at a good initial state. We may as well suppose that the switch is at the "ON" state with $\Delta\varphi = \pi$ induced by the thermo-optic effect, and the corresponding maximal transmissivity of the "bar" port is

$$T_{\mathrm{on}} = \frac{1}{4}\left[\sqrt{T_{1b}} + \sqrt{T_1}\right]^2 = 1, \quad (2)$$

where $T_{1t} = T_1(u_c) = 1$ and $T_2 = 1$ are, respectively, the transmissivity of the upper and bottom arms at the "ON" state. Further, by applying a switching voltage ($u_c = u_s$) to the p-i-n diode in the bottom arm, the MZI switch converts into the "OFF" state from the "ON" state, and the minimal transmissivity of the "bar" port becomes

$$T_{\mathrm{off}} = \frac{1}{4}\left[1 - \sqrt{\alpha_s}\right]^2, \quad (3)$$

where $\alpha_s = T_2(u_c = u_s)/T_2$ is the additional transmission coefficient of the bottom arm due to carrier injection. Therefore, at the ideal "ON" and "OFF" states, the ER of the optical switch has the maximum (intrinsic ER), expressed by $\mathrm{ER} = T_{\mathrm{on}}/T_{\mathrm{off}}$.

In fact, the refractive index and absorption coefficient of the bottom arm are determined by the carrier concentration. On the other hand, the process of carrier injection gives rise to joule heat and then the refractive index of the waveguide is changed by the thermo-optic effect. The "bar"-port transmissivity is dependent on the voltage u_c applied to the p-i-n diode, that is,

$$T(u_c) = \frac{1}{4}\left[1 + \alpha - 2\sqrt{\alpha}\cos(\pi + \Delta\varphi_c)\right], \quad (4)$$

where the additional transmission coefficient α is associated with excess loss induced by the FCA effect, and $\Delta\varphi_c = \Delta n_{\mathrm{eff}} k_0 l_c$ is the phase change at the applied voltage u_c, where k_0 and Δn_{eff} are the wave number and the effective refractive index change of the waveguide, respectively.

In what follows, the static and dynamic characteristics of the MZI optical switch are analyzed by simulation. According to the structure parameters of the p-i-n diode as mentioned above, the carrier concentration and the p-i-n diode temperature at different applied voltages are simulated by means of the DEVICE software (Lumerical Company) [20] and then the refractive index and absorption coefficient of the silicon waveguide can be calculated [21,22]. By using the MODE simulation software (Lumerical Company), we can further obtain the total effective refractive index change Δn_{eff} and the excess loss $\Delta L = -10 \lg \alpha$ of the silicon waveguide, as well as the separate contribution of the carrier concentration or the thermo-optic effect, $\Delta n_{\mathrm{eff},C}$ or $\Delta n_{\mathrm{eff},T}$, as shown in Fig. 2. It is well known that the effective refractive index change resulting from the thermo-optic effect increases with the applied voltage, contrary to that from the FCD effect. As a whole, the total effective refractive index decreases with the increase of the applied voltage. For the MZI switch with $l_c = 356$ μm, the "OFF" state can be implemented at the wavelength of 1550 nm when $\Delta n_{\mathrm{eff}} = -2.18 \times 10$, corresponding to the switching voltage of about 1.3 V and the excess loss of 1.82 dB ($\alpha_s = 0.66$).

The dynamic characteristics of the p-i-n diode can be investigated by means of $\Delta L(t)$, $\Delta n_{\mathrm{eff},C}(t)$, and $\Delta n_{\mathrm{eff},T}(t)$. When

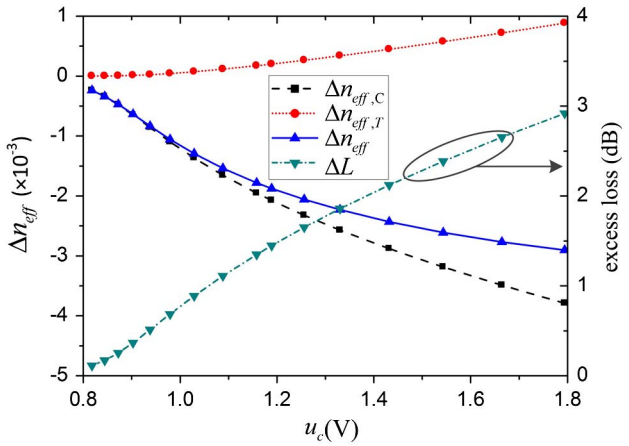

Fig. 2. Variations of the effective refractive index change and excess losses with the applied voltage.

the applied voltages rise steeply from 0 V to u_c, the optical switch starts to operate at the "OFF" state, and the above-mentioned parameters are of the exponential response as follows:

$$\Delta n_{\mathrm{eff},C}(t) = \Delta n_{\mathrm{eff},C}(\infty) \times [1 - \exp(-t/t_c)], \quad \textbf{(5a)}$$

$$\Delta L(t) = \Delta L(\infty) \times [1 - \exp(-t/t_c)], \quad \textbf{(5b)}$$

$$\Delta n_{\mathrm{eff},T}(t) = \Delta n_{\mathrm{eff},T}(\infty) \times [1 - \exp(-t/t_\theta)], \quad \textbf{(5c)}$$

where the time constants t_c and t_θ are, respectively, carrier lifetime and heat dissipation time ($t_c \ll t_\theta$), and the stable values at $t \to \infty$ are dependent on the applied voltage u_c. In turn, for the case from u_c to 0 V, the optical switch reverts to the "ON" state with the time responses as follows:

$$\Delta n_{\mathrm{eff},C}(t) = \Delta n_{\mathrm{eff},C}(0) \times \exp(-t/t_c), \quad \textbf{(6a)}$$

$$\Delta L(t) = \Delta L(0) \times \exp(-t/t_c), \quad \textbf{(6b)}$$

$$\Delta n_{\mathrm{eff},T}(t) = \Delta n_{\mathrm{eff},T}(0) \times \exp(-t/t_\theta), \quad \textbf{(6c)}$$

where the initial values at $t = 0$ are also dependent on the applied voltage u_c.

According to Eqs. (4)–(6), the dynamic characteristics of the optical switch can be calculated. Figure 3(a) shows the time response of transmissivity with $u_c = u_s = 1.3$ V and the dashed line represents the case without the thermo-optic effect, i.e., only the FCD effect is taken into account. In this paper, the switching duration of 2 μs is fixed in order to investigate the long-term stabilization process of the optical switch with the influence of the carrier injection and thermo-optic effect. From Fig. 3(a), the FCD effect is dominant over the thermo-optic effect when $t \ll t_\theta$; on the contrary, the thermo-optic effect plays an important role in the duration of $t \gg t_c$. For the case with $t \gg t_\theta$, the optical switch approaches an ideal "ON" or "OFF" level. Thus, strictly speaking, the transmissivity of the optical switch always lags behind the applied voltages to the p-i-n diode.

By comparison, if the thermo-optic effect is neglected in the carrier injection, the optical switch would rapidly operate at a stable state, as shown in Fig. 3(a). However, in that case the

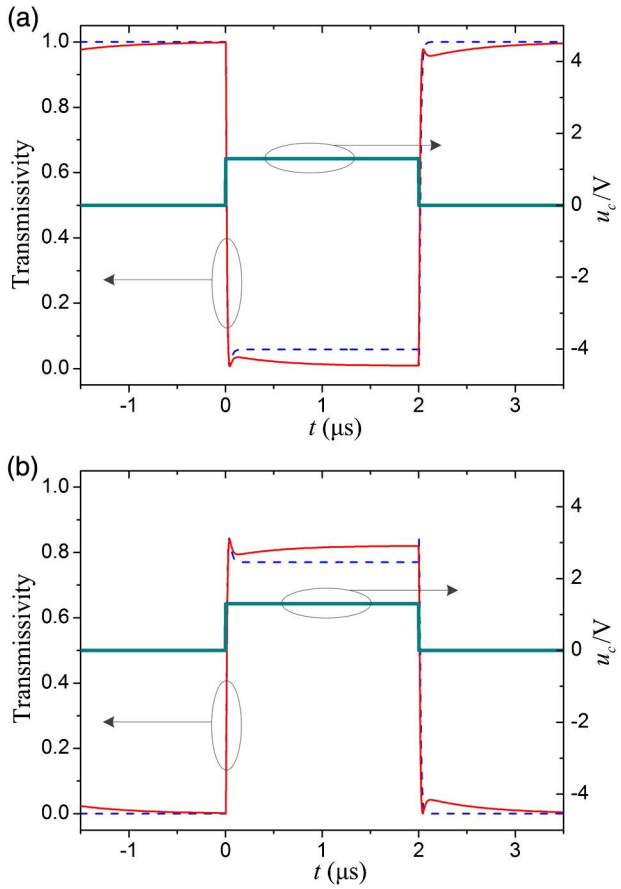

Fig. 3. Dynamic transmissivity of the optical switch with the applied voltage. (a) The "OFF" state is formed by carrier injection; (b) the "ON" state is formed by carrier injection. The dashed line represents the case in which the thermo-optic effect is neglected.

"OFF" state is defective because of larger transmissivity, which brings about the ER degradation.

According to the same analysis method presented above, Fig. 3(b) also gives the situation where the "ON" state is formed by carrier injection. The degradation of the thermo-optic effect on the switching performance is similar for the two cases. Without loss of generality, this paper will focus on the first case as shown in Fig. 3(a), where the carrier is injected through the p-i-n diode in the "OFF" state.

3. EXPERIMENTAL SETUP OF THE SILICON-BASED MZI OPTICAL SWITCH

The experimental platform used here is based on a 4 × 4 silicon-based optical switching chip, composed of six 2 × 2 MZI optical switches of the Benes structure. The electrodes of the p-i-n diodes and the silicon resistive heaters integrated in the two arms of the MZI switch are wire-bonded to a chip plug base. We developed a programmable FPGA-based driver circuit for supplying the proper voltages to the p-i-n diodes and resistive heaters. The drive circuit has a low output voltage jitter of less than 2% and the voltages applied to the p-i-n diodes are in the range of 1.2–1.4 V for the "OFF" states. For convenience, the 4 × 4 silicon-based optical switching chip is also packaged

into an optical module coupled through the input and output array fibers. The experimental setup is illustrated in Fig. 4. For all 24 switching states, the measured fiber-to-fiber insertion losses are in the range of 23–26 dB, with the maximal crosstalk of −12 dB.

As an example, we investigated the dynamic characteristics of a last-order 2 × 2 MZI optical switch, while the other 2 × 2 MZI optical switches are kept fixed in the experiment, as shown in Fig. 4. The 1550 nm continuous-wave light is coupled into the input port I_1 of the chip module through a fiber polarization controller (FPC), and the optical waveform from the output port O_1 is detected with an avalanche photodiode. The measured switching waveforms under the control of different square-wave voltage signals with the pulse width of 2 μs are shown in Fig. 5. By comparing Fig. 3 with Fig. 5, the theoretical curve is identical with the experimental waveform at the applied voltage of 1.3 V, and the measured ER under stable state is 18.4 dB, with the fitting time constants $t_c \approx 10$ ns and $t_\theta \approx 0.6$ μs. As we can see here, the carrier lifetime is much smaller than heat dissipation time, resulting in a much faster switching speed than that of the thermo-optical switches, so that the silicon-based EO switches are regularly working at the nanosecond order. However, in order to study in the long-term stabilization of the carrier injection with the influence of the thermo-optic effect, the configuration time is set in the order of microsecond, even though it is much smaller in practical applications.

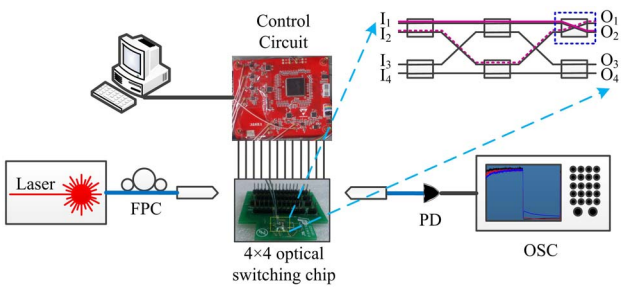

Fig. 4. Experiment setup. FPC, fiber polarization controller; PD, photodetector; OSC, oscilloscope.

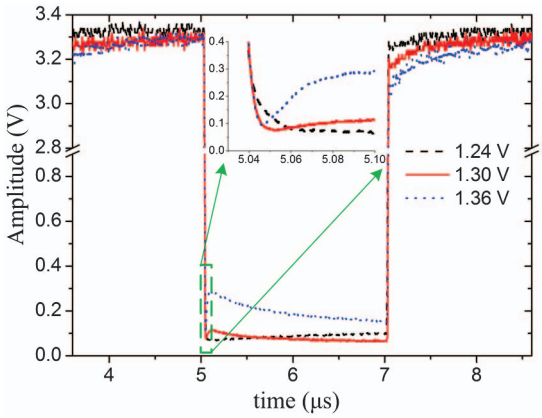

Fig. 5. Output switching waveforms under different applied voltages. Inset shows the close-up plot of the first ∼100 ns when the voltage is applied to the switch.

In the traditional driving scheme, the optimal voltage applied to the p-i-n diode is corresponding to the maximum stable ER in practice, and the driven voltages applied to the p-i-n diode and the resistive heater are, respectively, $u_s = 1.30$ V and $u_t = 5.49$ V in this experiment. From Fig. 5, the output waveform has a light distortion when $u_s = 1.30$ V; when $u_c = 1.24\ \text{V} < u_s$, the thermo-optic effect in carrier injection can give rise to a slow increase of the output optical power at the "OFF" state, and then the stable ER is degraded by 4 dB, regardless of small waveform distortion. It should be pointed out that the traditional driving scheme has two shortcomings as follows: (1) the existence of the waveform distortion restricts the switching time to some extent, and (2) a larger carrier concentration is required to balance the thermo-optic effect, which will reduce the stable ER due to larger excess loss induced by FCA.

4. SYNCHRONOUS DRIVING SCHEME

To further improve the switching performance, we propose a synchronous driving scheme, in which the resistive heater on one arm of each 2 × 2 MZI switch is driven by a synchronously

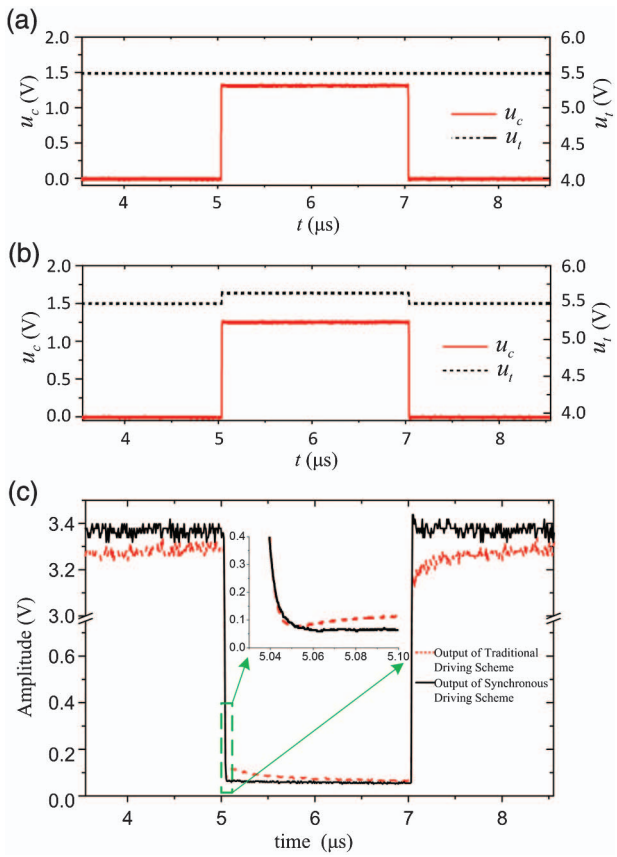

Fig. 6. Comparison between the traditional and synchronous driving schemes. (a) Applied voltage signals in the traditional driving scheme. (b) Applied voltage signals in the synchronous driving scheme. (c) Output waveforms of the traditional (red line) and synchronous (black line) driving schemes. Inset shows the close-up plot of the first ∼100 ns when the voltage is applied to the switch.

modulating signal, varying with the on–off voltages applied to the p-i-n diode on the other arm. Figure 6 gives the output waveforms from the optical switch and the corresponding applied voltages in the traditional and synchronous driving schemes. Just as is done in the traditional driving schemes, in the synchronous driving schemes, the driven silicon resistive heater and p-i-n diode are, respectively, positioned on the upper and bottom arms of the MZI optical switch, and the driven voltages applied to the p-i-n diode and the resistive heater become $\tilde{u}_s = 0/1.24$ V and $\tilde{u}_t = 5.49$ V/5.63 V, respectively. It should be mentioned that the input power in our driving scheme is slightly higher than that in the traditional scheme, so as to clearly show the difference between the output waveforms of the two schemes. From Fig. 6, when the silicon resistive heater is driven by a synchronously modulating signal instead of a fixed-bias voltage, a synchronous thermal compensation for the carrier injection process can be realized and then bring about a better output waveform. Meanwhile, the stable ER is also improved by 1 dB due to a smaller operating voltage.

We also measured the stable ERs at the different voltages applied to the p-i-n diode for the two driving schemes, and the drive voltage applied to the silicon resistive heater is always optimized so that the phase difference is $\Delta\varphi = 0$ in each test, as shown in Fig. 7(a). For the synchronous driving scheme, our experimental results show that the stable ER, as well as the output waveform, can be improved when u_c decreases to 1.24 V from 1.3 V; however, the deterioration of the output waveform occurs with smaller $u_c (< 1.24$ V) in spite of having a larger stable ER. In fact, it passes through three stages, those of thermal under-, critical-, and over-compensation, which can theoretically be explained by means of Fig. 7(b). For the traditional driving scheme, the calculated curves I in Fig. 7(b) are basically identical with the experimental results in Fig. 7(a), in which the electro-optic effect (including the FCD and FCA effect) and the thermo-optic effect are considered in our calculation. By comparison, curves II and III in Fig. 7(b) are, respectively, the cases that the thermo-optic effect in the p-i-n diode is neglected and only the FCA effect is considered while the phase difference is $\Delta\varphi = 0$. From Fig. 7, curve III is compatible with the experimental data obtained in the synchronous driving scheme, as in the synchronous driving scheme the thermal compensation will always make the transmissivity minimal, which means the same condition with curve III. In a word, the synchronous driving scheme is capable of providing a critical thermal compensation for the thermo-optic effect in carrier injection and further improving the stable ER of the MZI optical switches.

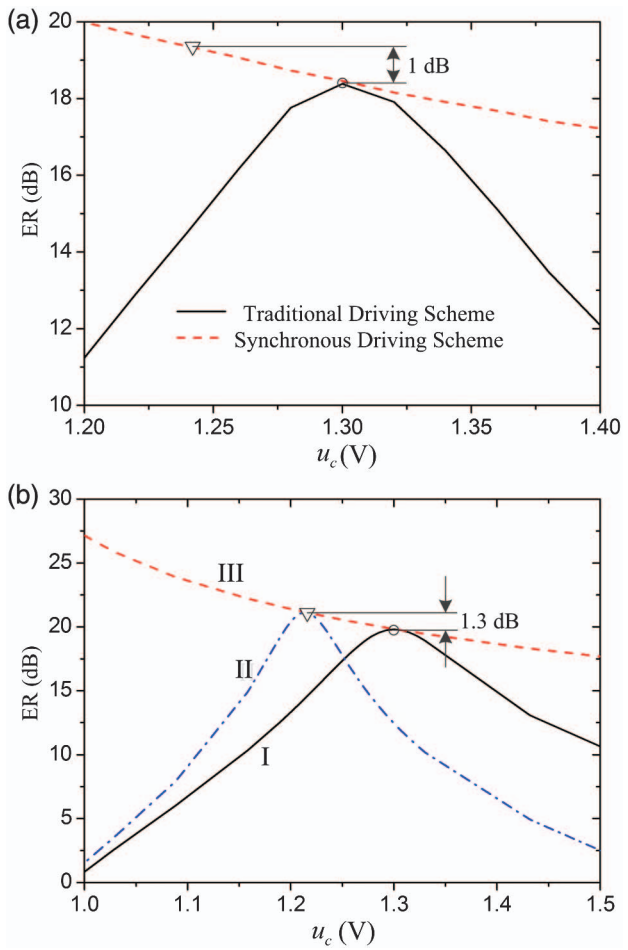

Fig. 7. Experimental (a) and calculated (b) ER curves for the two driving schemes.

5. CONCLUSION

The thermo-optic effect in carrier injection p-i-n diode silicon-based optical switches is significant, which will cause waveform distortion and ER reduction. A 1 dB ER improvement, along with a better output waveform, is achieved with the proposed synchronous driving scheme, which is capable of critically compensating for the temperature variation thanks to the same structure being shared by the p-i-n diode and the silicon resistive heater. It is worth mentioning that the effectiveness of the proposed driving method on 20 ns in optical packet switching networks might be cut down due to the low thermal response, and further research needs to be done in the future. Still, we believe that the proposed synchronous driving scheme has a potential application in large-scale optical-integrated switches.

Funding. National 863 Program of China (2013AA014402); National Natural Science Foundation of China (NSFC) (61271166, 61505021); Fundamental Research Funds for the Central Universities (ZYGX2014J005); Program for Changjiang Scholars and Innovative Research Team in University.

REFERENCES

1. A. Shacham, K. Bergman, and L. P. Carloni, "Photonic networks-on-chip for future generations of chip multiprocessors," IEEE Trans. Comput. **57**, 1246–1260 (2008).
2. R. G. Beausoleil, M. McLaren, and N. P. Jouppi, "Photonic architectures for high-performance data centers," IEEE J. Sel. Top. Quantum Electron. **19**, 3700109 (2013).
3. A. V. Rylyakov, C. L. Schow, B. G. Lee, W. M. J. Green, S. Assefa, F. E. Doany, M. Yang, J. V. Campenhout, C. V. Jahnes, J. A. Kash, and Y. A. Vlasov, "Silicon photonic switches hybrid-integrated with CMOS drivers," IEEE J. Solid-State Circuits **47**, 345–354 (2012).
4. C. Sun, M. T. Wade, Y. Lee, J. S. Orcutt, L. Alloatti, M. S. Georgas, A. S. Waterman, J. M. Shainline, R. R. Avizienis, S. Lin, B. R. Moss, R. Kumar, F. Pvanello, A. H. Atabaki, H. M. Cook, A. J. Ou, J. C. Leu,

Y. H. Chen, K. Asanovic, R. J. Ram, M. A. Popovic, and V. M. Stojanovic, "Single-chip microprocessor that communicates directly using light," Nature **528**, 534–538 (2015).
5. P. De Dobbelaere, K. Falta, S. Gloeckner, and S. Patra, "Digital MEMS for optical switching," IEEE Commun. Mag. **40**(3), 88–95 (2002).
6. M. Mizukami, J. Yamaguchi, N. Nemoto, Y. Kawajiri, H. Hirata, S. Uchiyama, M. Makihara, T. Sakata, N. Shimoyama, and K. Oda, "128 × 128 three-dimensional MEMS optical switch module with simultaneous optical path connection for optical cross-connect systems," Appl. Opt. **50**, 4037–4041 (2011).
7. R. Kasahara, M. Yanagisawa, T. Goh, A. Sugita, A. Himeno, M. Yasu, and S. Matsui, "New structure of silica-based planar lightwave circuits for low-power thermooptic switch and its application to 8 × 8 optical matrix switch," J. Lightwave Technol. **20**, 993–1000 (2002).
8. T. Shibata, M. Okuno, T. Goh, T. Watanabe, M. Yasu, M. Itoh, M. Ishii, Y. Hibino, A. Sugita, and A. Himeno, "Silica-based waveguide-type 16 × 16 optical switch module incorporating driving circuits," IEEE Photon. Technol. Lett. **15**, 1300–1302 (2003).
9. P. Dong, S. Liao, H. Liang, R. Shafiiha, D. Feng, G. Li, X. Zheng, A. V. Krishnamoorthy, and M. Asghari, "Submilliwatt, ultrafast and broadband electro-optic silicon switches," Opt. Express **18**, 25225–25231 (2010).
10. J. Van Campenhout, W. M. J. Green, S. Assefa, and Y. A. Vlasov, "Low-power, 2 × 2 silicon electro-optic switch with 110-nm bandwidth for broadband reconfigurable optical networks," Opt. Express **17**, 24020–24029 (2009).
11. T. Chu, L. Qiao, and W. Tang, "High-speed 8 × 8 electro-optic switch matrix based on silicon PIN structure waveguides," in *12th International Conference on Group IV Photonics (GFP)* (2015), pp. 123–124.
12. H. Zhou, M. Liao, S.-W. Huang, L. Zhou, K. Qiu, and C. W. Wong, "Six-wave mixing induced by free-carrier plasma in silicon nanowire waveguides," Laser Photon. Rev. **10**, 1054–1061 (2016).
13. L. Lu, S. Zhao, L. Zhou, D. Li, M. Wang, X. Li, and J. Chen, "16 × 16 non-blocking silicon optical switch based on electro-optic Mach-Zehnder interferometers," Opt. Express **24**, 9295–9307 (2016).
14. M. Yang, W. M. J. Green, S. Assefa, J. Van Campenhout, B. G. Lee, C. V. Jahnes, F. E. Doany, C. L. Schow, J. A. Kash, and Y. A. Vlasov, "Non-blocking 4 × 4 electro-optic silicon switch for on-chip photonic networks," Opt. Express **19**, 47–54 (2011).
15. B. G. Lee, A. Rylyakov, W. M. J. Green, S. Assefa, C. W. Baks, R. Rimolo-Donadio, D. Kuchta, M. Khater, T. Barwicz, C. Reinholm, E. Kiewra, S. Shank, C. Schow, and Y. A. Vlasov, "Monolithic silicon integration of scaled photonic switch fabrics, CMOS logic, and device driver circuits," J. Lightwave Technol. **32**, 743–751 (2014).
16. L. Zhou, X. Zhang, L. Lu, and J. Chen, "Tunable vernier microring optical filters with p-i-p type microheaters," IEEE Photon. J. **5**, 6601211 (2013).
17. Z. Jiate, Z. Yong, W. Wanjun, H. Uinlei, Z. Qiang, Y. Jianyi, W. Minghua, and J. Xiaoqing, "Analysis of the thermo-optic effect in lateral-carrier-injection SOI ridge waveguide devices," J. Semicond. **31**, 064009 (2010).
18. L. Lu, L. Zhou, Z. Li, X. Li, and J. Chen, "Broadband 4 × 4 non-blocking silicon electro-optic switches based on Mach-Zehnder interferometers," IEEE Photon. J. **7**, 7800108 (2015).
19. L. Lu, L. Zhou, X. Li, and J. Chen, "Low-power 2 × 2 silicon electro-optic switches based on double-ring assisted Mach-Zehnder interferometers," Opt. Lett. **39**, 1633–1636 (2014).
20. Lumerical, "Lumerical product overview," https://www.lumerical.com/tcad-products/.
21. R. A. Soref and B. R. Bennett, "Electrooptical effects in silicon," IEEE J. Quantum Electron. **23**, 123–129 (1987).
22. A. W. Poon, X. Luo, F. Xu, and H. Chen, "Cascaded microresonator-based matrix switch for silicon on-chip optical interconnection," Proc. IEEE **97**, 1216–1238 (2009).